SI Appendix

Directionally-biased sidestepping of Kip3/kinesin-8 is regulated by ATP waiting time and motor-microtubule interaction strength

Aniruddha Mitra[a,b], Felix Ruhnow[a, c], Salvatore Girardo[d], Stefan Diez[a,b,e]

[a] B CUBE - Center for Molecular Bioengineering, Technische Universität Dresden, Arnoldstraße 18, 01307 Dresden, Germany
[b] Center for Advancing Electronics Dresden (cfaed), Technische Universität Dresden, Helmholtzstraße 18, 01069 Dresden, Germany
[c] Current address: School of Biosciences, University of Melbourne, Parkville, VIC 3010, Australia
[d] Biotechnology Center, Center for Molecular and Cellular Bioengineering, Technische Universität Dresden, Tatzberg 47/49, 01307 Dresden, Germany
[e] Max Planck Institute of Molecular Cell Biology and Genetics, Pfotenhauerstraße 108, 01307 Dresden, Germany

Kip3-mfGFP expression and purification

The Kip3 cDNA was inserted in the commercially available baculovirus transfer plasmid pOET1 (Oxford Expression Technologies, UK). One HindIII restriction site was removed from Kip3 cDNA without changing the amino acid sequence by site-directed mutagenesis. mfGFP sequence was amplified via PCR and restriction sites AscI and HindIII were inserted. The sequence was then inserted into the pOET1-Kip3 using AscI and HindIII restriction enzymes (New England Biolabs). The Kip3-mfGFP construct was expressed in Sf+ cells (Invitrogen, Paisley, UK) and harvested for 3 days. The cells were pelleted, washed and resuspended in Kip3 buffer (25 mM Tris HCl [VWR], pH 7.4 adjusted with KOH [VWR], 300 mM NaCl [VWR], 5 mM Imidazole [Sigma], 5 mM $MgCl_2$ [VWR], 0.2% Triton X-100 [Sigma], 10% glycerol [VWR], 10 mM DTT [Thermo Scientific, Waltham, USA] and 1mM ATP [Jena Bioscience GmbH, Jena, Germany]) along with an EDTA-free protease inhibitor cocktail (Complete Ultra Tablets, Sigma). All following steps were performed at 4°C. The cells were lysed by centrifugation for 1h at 40,000g. For purification of the Kip3-mfGFP protein the cell lysate was incubated with Ni-NTA agarose (Qiagen) for 2h, washed several times in a 10ml column (Bio-Rad) with Kip3 buffer (with additional 30-50mM imidazole) and eluted with Kip3 buffer containing 150mM imidazole. Eluted protein was snap-frozen in liquid nitrogen and stored at -80°C.

Fabrication of polymer structures on glass

The strategy used for fabrication of the patterned glass coverslips is described briefly: (i) The pattern to be imprinted was designed and printed on a chrome photomask (JD Photo Data, Herts, UK). (ii) The Master was fabricated by photolithography by using a mask aligner (EVG, EVGroup, St. Florian am Inn, Austria). Exactly a 4'' silicon wafer coated with a positive photoresist (AZ 9260; MicroChemicals GmbH, Ulm, Germany), 1:3 (w/w)

diluted in PGMEA (MicroChemicals GmbH), was irradiated by UV light (100 mJ/cm^2) through the photomask and developed in AZ400K (MicroChemicals GmbH). The surface was then spin-coated with an anti-sticking layer (ASL; EVGroup). (iii) 3 gr perfluoropolyether (PFPE; Fluorolink MD700, Solvay, Milan, Italy) mixed with 6 mg of a cross-linker (Irgacure 2022; BTC Europe GmbH, Köln, Germany) was poured on the master surface. A glass substrate, functionalized with KBM primer (EVGroup) to improve polymer adhesion, was pressed on top of the liquid. (iv) After liquid spreading, the sandwich structure was exposed to UV light (5000 mJ/cm^2) to polymerize the liquid. (v) The glass substrate was peeled off from the master (the ASL layer on the master promotes easy release of the stamp from the master). The final stamp is a glass surface coated with the patterned (negative of the master) PFPE polymer. (vi) An easy-cleaned (1) glass coverslip (22×22 mm^2) was spin-coated with an adhesion promoter, EVGprime/ZAP 1020 (height 10 nm; EVGroup) and with an UV curable resin, EVG NIL UV/A 200nm (height 280 nm; EVGroup). (vii) A mask aligner (EVG 620; EVGroup), equipped with tools for the UV Nanoimprint Lithography (UV-NIL) process, was used to control the alignment and to adjust the pressure between the stamp and the coated coverslip. (viii) Resin crosslinking was activated by UV exposure (2500 mJ/cm^2). The applied pressure (1 bar) ensures the filling of the hollow space in the stamp (avoids the formation of air bubbles) leading to a perfect negative copy of the structures from the stamp. (ix) Finally, the coverslip with the desired resin pattern was peeled off from the stamp.

3D single molecule imaging set-up, Parallax

In our Parallax set up (adapted from Sun et al. (2)) we split the beam path at the Fourier plane (a plane conjugate to the objective back focal plane) and acquired both the split images simultaneously. The basic principle is illustrated in Fig. S3A. When the beam path is split along the y-axis (or x-axis) in the Fourier plane, the point spread function (PSF) corresponding to each light emitting probe at the image plane is split into half creating two antagonistic PSFs asymmetric along the y-axis. For a regular PSF of an image in focus, any motion out of focus in z direction results in the spreading of the PSF. However, the central position determined from the peak of the Gaussian fitted to the PSF does not change and we obtain no information regarding the z direction. In case of Parallax the two asymmetric PSFs corresponding to an image in focus also spread with movement of the image out of focus in the z direction. However, since the PSFs are asymmetric along the y-axis, the central position of the PSFs shift in y direction and the relative change in y (Δy) between the two PSFs is proportional to the shift of the image in z.

In our set-up (Fig. S3B) we used a commercially available D-shaped mirror (all optical elements from Thorlabs) to split the image beam path. A lens (f = 150 mm; L1) was placed one focal length away from the image plane, which collimates the beam flux coming from the image. The beam flux was then split using a sharp-edged D-shaped mirror (D1) that

was positioned such that half the beam could pass through while the other half gets reflected. Both the beams were guided to the camera chip (referred to as new image plane) using mirrors (R1, R2 and D2) and focusing lens (L2 and L3; f = 200 mm) to form the two split images. The two split images were recorded simultaneously on the upper and lower halves of the camera chip. In this set-up, when an optical probe moves only in the xy plane, both the acquired split images move the same amount in the x and y directions. However, when the probe moves out of focus in the z-direction, the acquired split images move towards or away from each other in the y direction (as seen for an example 200nm Tetraspeck bead in Fig. S3C).

In order to obtain the 3D coordinates of the optical probes, acquired image streams were analyzed using FIESTA (3) where every frame was split laterally into two halves (corresponding to the two split images created by the Parallax setup) to create separate image channels. The track coordinates for each optical probe was obtained in the two split channels. The x and y coordinates for the final 3D track corresponding to an optical probe was calculated by averaging the x and y coordinates (absolute) of the track in the two split channels while the z coordinates were obtained from the relative difference in the y coordinates (Δy) multiplied by a certain z position conversion factor. To calculate the conversion factor, Tetraspeck beads (attached unspecifically to a glass surface; N = 49) were imaged using Parallax at 10 fps over a Piezo-stage (Mad City Labs Inc., Madison, USA) moved in the z direction by 20 nm steps every 5 s. Assuming a linear response of Δy to z-shift, a mean step-size of 8.8 ± 2 nm corresponding to the 20 nm steps provided a z position conversion factor of 2.3.

The localization error for tracking Kip3-QDs was about 20 nm in each dimension. Though being roughly twice as big as the localization error reported for Kip3 motors labeled with QDs at their motor domains, using total internal reflection (TIRF) microscopy on glass coverslips (4) this value is well conceivable when considering (i) the flexibility of the Kip3 tail that binds to the QD, (ii) the reduced optical contrast in highly incline thin illumination microscopy (HILO (5)) used in our assay vs. TIRF illumination, (iii) the residual autofluorescence and absorption of the polymer structures, (iv) the scattering of the optical components in the Parallax setup, and (v) the likely residual thermal motion of the suspended microtubules.

Microtubule preparation

Porcine tubulin was purified from porcine brain (Vorwerk Podemus, Dresden, Germany) using established protocols as described previously (6). For the speckle-FLIC gliding assays, Guanylyl-(α,β)-methylene-diphosphonate (GMP-CPP) grown, taxol-stabilized rhodamine speckled microtubules were grown as described in Mitra et al (7). For the suspended microtubule stepping assays, long (average length ≥ 15 μm), GMP-CPP grown, taxol-stabilized (double-stabilized) rhodamine labeled microtubules were produced in the following manner: 100 μl of BRB80 solution (80 mM Pipes [Sigma], pH

6.9 adjusted with KOH [VWR], 1mM EGTA [Sigma], 1 mM $MgCl_2$ [VWR]) supplemented by 2 µM *porcine* tubulin (1:3 mixture of rhodamine-labeled [TAMRA; Thermo Fisher Scientific] and unlabeled), 1 mM GMP-CPP (Jena Bioscience, Jena, Germany) and 1mM $MgCl_2$ were incubated on ice for 5 minutes, before polymerization for 15-20 h at 27 °C to obtain long microtubules. Free tubulin was removed by centrifuging the solution using a Beckman airfuge (Beckman, Brea, CA) at 100,000g for 5 min. The pellet was resuspended in a volume of 50-100 µl BRB80T (BRB80 supplemented with 10 µM Taxol [Sigma]). For cleavage of the microtubule e-hooks, rhodamine speckled microtubules were incubated with 100-200 µg/ml subtilisin (Sigma) for 40 min at 37 °C. The reaction was stopped by subsequently adding 10 mM PMSF (Sigma) to the microtubule solution. The digested microtubules were centrifuged and the pellet was resuspended in 50 µl BRB80T.

In vitro motility assays

Kip3-QD stepping assays on suspended microtubules: All Kip3-QD stepping assays were performed in microfluidic flow channels constructed on 22 × 22 mm^2 glass coverslips (#1.5; Menzel, Braunschweig, Germany) patterned with UV-NIL polymer resin and 18 ×18 mm^2 unpatterned glass coverslips, both dichlorodimethylsilane-coated to make the surface hydrophobic, as described in Korten et al. (8). Before silanization, the patterned coverslips were only cleaned mildly (sonicated in 5 % mucasol [VWR] and then in 70% ethanol [VWR]) to avoid corrosion of the structure. Typically, each coverslip had three flow channels having the dimensions of 18 mm × 3 mm × 100 µm (L × W × H). Control Kip3 stepping assays and Kip3-QD stepping assays were performed on unpatterned silanized coverslips as described in Korten et al. (8). Flow channels were flushed with a sequence of: (i) Bead solution consisting of 0.5 % 200 nm Tetraspeck beads (Invitrogen) in PBS (incubation time 1 min). (ii) Antibody solution consisting of 3 mg/ml anti-beta tubulin antibody (SAP.4G5; Sigma) in PBS in order to unspecifically bind antibodies to the surface (incubation time 5 min). (iii) Pluronic F127 (1 % in PBS; Sigma) in order to block the surface from unspecific protein adsorption (incubation time >60 min). (iv) 4x BRB80 buffer to remove excess F-127 in solution and to exchange buffers. (v) Microtubule solution with high concentration of microtubules in BRB80T, followed by an immediate washing step with BRB80T in order to immobilize microtubules perpendicular to the ridges via specific interactions with anti-beta tubulin antibodies. (vi) Imaging solution consisting of 112.5 mM KCL, 1 mM ATP (varied between 1 µM to 1 mM for the experiment to measure ATP dependence on Kip3 velocity), 0.1 % Tween20 [Sigma], 0.2 mg/ml casein, 0.2 mg/ml DTT, 10 µM Taxol and an oxygen scavenger mixture (consisting of 40 mM glucose [Sigma], 110 µg/ml glucose oxidase [SERVA], 22 µg/ml catalase [Sigma]) in BRB80 for imaging microtubules in order to find a suitable field of view. (vii) Kip3-QD buffer consisting of Kip3-QD conjugate solution diluted 100 times in imaging solution. The Kip3-QD conjugate solution consists of 100 nM QD (QD 655 Streptavidin conjugate; Invitrogen) and 10 nM Kip3-mfGFP (at 10:1 conjugation ratio, unless specified otherwise),

incubated in motor dilution buffer (imaging solution without the oxygen scavenger system) for >30 min.

Control Kip3 stepping assays: In control Kip3 stepping assays a similar protocol (besides the following alterations) was used: (i) the bead solution consisted of 0.1 % 100 nm Tetraspeck beads (Invitrogen) in PBS and (ii) the concentration of the unconjugated Kip3 motors in the imaging solution was 0.04 nM.

Kip3 gliding assays: Kip3 gliding assays were performed in microfluidic flow channels constructed from hydrophobic glass coverslips and silicon wafers with a 30nm thermally grown oxide layer (GESIM, Grosserkmannsdorf, Germany) as described in Mitra et al. (7). The ATP concentration was 1 mM and the KCl concentration was 112.5 mM unless indicated otherwise. For the phosphate salt experiments, 112.5 mM KCl was replaced by 112.5 mM KP_i (50 % monobasic, 50 % dibasic; Merck) in the imaging solution.

Wild-type kinesin-1 and Kinesin-1_{+DAL} gliding assays: Wild-type kinesin-1 gliding assays were performed on silicon wafers with a 30 nm thermally grown oxide layer as described in Nitzsche et al. (9). *Kinesin-1_{+DAL}* gliding assays were performed similar to Kip3 gliding assays except for the following changes: (i) The motors were specifically bound to the surface via Penta-His antibodies (Qiagen) instead of GFP antibodies. (ii) No additional KCl was added to the buffer. In both the assays, the ATP concentration was varied as indicated in the results.

Considerations for stepping assays on suspended microtubules.

- Microtubules were introduced into the channels in high density and immediately washed out to ensure that they attach perpendicular to the ridges in a taut manner. However, due to the blunt profile, microtubules were often not suspended tautly, but slacked in the middle. It was therefore necessary to have 250 nm high ridges (100 nm ridges were found to be too shallow with majority of the microtubules touching the valley surface) for double-stabilized microtubules so that the microtubules did not interact with the valley surface (the height needs to be even more for GTP grown taxol stabilized microtubules which have a persistence length 3 times lower than the double-stabilized microtubules (10)).
- The slacking of microtubules in the middle was significant for microtubules not bound rigidly to the ridges. Therefore, the ridges were 2 (or 5 µm) wide and excess of anti-tubulin antibodies were applied (in comparison to the amount used in conventional stepping assay (8)) to ensure ample attachment points for microtubules.
- The polymer resin patterned on the glass coverslips had some autofluorescence signal that was bleached before introducing the Kip3-QDots in the stepping motility assays, in order to minimize the background noise.

- Since the ridges were 250 nm high, total internal reflection fluorescence microscopy (TIRF) was not a viable option to image the Kip3-QDots. In order to reduce the background noise due to QDots in the solution, the Kip3-QDots were imaged using HILO (5).

Image acquisition

Kip3-QD stepping assays on suspended microtubules: Optical imaging was performed using an inverted fluorescence microscope (Axio Observer Z1; Carl Zeiss Microscopy GmbH, Jena, Germany) with a 63x oil immersion 1.46NA objective (Zeiss) in combination with an EMCDD camera (iXon Ultra; Andor Technology, Belfast, UK) controlled by Metamorph (Molecular Devices Corporation, Sunnyvale, CA, USA). For 3D imaging, a custom built optical setup called Parallax (2) (SI Appendix, Fig. S3 and 3D single molecule imaging set-up, Parallax), was placed in the image beam path between the inverted fluorescence microscope and the EMCCD camera. Temperature (24 °C) was controlled by fitting a custom made hollow brass ring around the body of the objective and connecting it to a water bath with a cooling/heating unit (F-25-MC Refrigerated/Heating Circulator; JULABO GmbH, Seelbach, Germany) (11). Rhodamine-labeled microtubules were observed by epifluorescence using a metal arc lamp (Lumen 200; Prior Scientific Instruments Ltd., Cambridge, UK) with a TRITC filter (ex BL520/35, dc zt532 RDCXT, em BL585/40; all Chroma Technology Corp., Rockingham, VT). QD signal from the Kip3-QD conjugates were observed in HILO mode (5) using a PhoxX 488 nm Laser (≈ 15-30 mW; Omicron-Laserage, Rodgau-Dudenhofen, Germany) with a QD655 filter set (ex BL475/35, dc zt488 RDC, em BL655/40; all Chroma). For control Kip3 stepping assays a different EMCCD (iXon3; Andor Technology) was used and the GFP signal from the Kip3-mfGFP motors was observed in total internal reflection (TIRF) mode using the PhoxX 488 nm Laser with a GFP filter set (ex BL475/35, dc zt 488 RDC, em BL525/35; all Chroma). In suspended microtubule stepping assays, reference beads and rhodamine-labeled double-stabilized microtubules were immobilized on the polymer-patterned coverslips and the split images were observed simultaneously on two halves of the same camera chip. A field of view was selected when there were 3 (or more) reference beads bound to the surface and numerous microtubules suspended between ridges. The microtubules were imaged for 100 frames (5 fps) in order to eliminate evaluation of Kip3-QD events on swiveling microtubules or microtubules touching the valley surface (interpreted qualitatively from the difference in the microtubule profile in the two split images). The region was then exposed to 488 nm laser light (excitation light used later for imaging the QDs) for 1-2 min to bleach the background autofluorescence signal from the polymer-pattern. Afterwards, the QD-Kip3 mixture was flushed in and image acquisition (3-5 fps) was started after 1min in order to record QD-Kip3 motility events.

Gliding assays: Optical imaging was performed using an inverted fluorescence microscope with a 63x water immersion 1.2NA objective (Zeiss) in combination with an

EMCCD (iXon3) camera controlled by Metamorph. A metal arc lamp (Lumen 200) was used for epifluorescence excitation. Rhodamine-speckled microtubules gliding on the silicon-wafer surfaces were imaged “through the solution” (i.e. on the far side of the flow channels) using the TRITC filterset with an exposure time of 400 ms per frame. Images were recorded in time-lapse mode (0.2-1 fps). Temperature (24 °C) was maintained (or varied in case of experiments at different temperatures) in the same manner as for the stepping assays. For the wild-type kinesin-1 and KDAL-560 gliding assays, the frame rate was adjusted to 0.1- 10 fps depending on the gliding speeds.

Image analysis

Kip3-QD stepping assays on suspended microtubules: The acquired image stream of the Kip3-QD stepping assay was analyzed using FIESTA (3) where every frame was split laterally into two halves, corresponding to the two split images created by the Parallax setup (2) (described in SI Appendix, 3D single molecule imaging set-up, Parallax), to create separate image channels. Since the split beam paths cannot be projected exactly onto the two halves of the camera chip (due to limitations in the alignment of the optical elements), a translational and rotational offset between the two channels was obtained by the reference beads (minimum 3 reference points necessary). Stage drift during imaging was corrected with the averaged position of the reference beads (in 3D). Each Kip3-QD event was tracked in the two channels and coordinates (in 3D; see SI Appendix, 3-D single molecule imaging set-up, Parallax) were obtained (offset and drift corrected). The coordinates were fitted around a tube of diameter 25 nm (to account for microtubule width) using spline interpolation to obtain angular information of the Kip3-QD track with respect to the microtubule (see SI Appendix, Fitting of Kip3-QDot tracks section for details). In order to obtain the rotational pitch of the track, the angular information for the Kip3-QD event was plotted against the travelled distance and the rotational pitch as well as the end-to-end velocity for each rotation was derived by manual computer-aided measurement. For calculation of the effective sidestepping rate as well as effective sidestepping probability we used the 8.4 μm supertwist (7) and 8.3 nm tubulin interdimer distance for GMPCPP microtubules (see SI Appendix, Calculation of stepping parameters for details). For obtaining velocities in control Kip3 stepping assays, the stepping events were tracked using FIESTA (3) and the slope of the linear fit of the distance-time information provided the velocity (11).

Gliding assays: The rotational pitch of the gliding speckled microtubules was obtained from their kymographs (space-time intensity plots), which were generated in ImageJ (12). The kymographs were then analyzed with MATLAB (Mathworks, Natick, MA) using the speckle analysis method described in Mitra et al. (7).

Selection criteria for further analysis of Kip3-QDot tracks.

- Tracks smaller than 3000 nm were ignored.
- Tracks on fluctuating microtubules or microtubules interacting with the valley surface were ignored. Such microtubules were identified by imaging the microtubules before adding the Kip3-QDot conjugates and detecting floppy swiveling microtubules (occurs if the microtubules are not rigidly bound to the ridges) or microtubules having an unusual profile (probably due to interaction with the valley surface).
- Tracks with very large displacements (> 500 nm between frames) possibly obtained on microtubules that were displaced while imaging the QDot signal were also eliminated.
- Tracks with large and/or frequent gaps were also ignored. Such tracks were obtained for Kip3-QDot conjugates having one or more of the following issues; (1) poor signal-to-noise ratio (2) blinking (undergoing fluorescence intermittency) very frequently (3) too close to reference beads (4) too close to other Kip3-QDot conjugates.

Fitting of Kip3-QDot tracks

The Kip3-QDot track data was fitted to a spline (a spline is a piecewise cubic curve bent to pass through a number of predefined points referred to as “knots”) using non-linear least-squares fitting. 4 knots were placed along the QDot-Kip3 track that includes the start and end point of the track and 2 additional roughly equidistant points (to each other as well as to the start and end points) along the track (the number of knots can be reduced or increased to account for the flexibility of the microtubule). The x-position of the first and last knots were kept constant (since the maximum displacement is always along the x-axis), while all other positions were varied to find the optimal path with least square fitting. The x-position of the inner knots was restricted within the x-position of the start and end points. A cubic spline along the knots was interpolated in all three dimensions and the minimum distance to the spline was calculated. In addition, instead of using a regular spline, a tube around the spline with a radius of 12.5 nm was used to account for the microtubule width. Minimum distance of each tracked data point from the surface of the fitted tube was calculated by subtracting 12.5 nm from the minimum distance to the spline and because negative values denote points within the tube they were replaced with their absolute values multiplied by 5 (as a penalty to make their contribution less significant when optimizing the fitted path). The points of the track were then projected on the optimized path and the angle of the Kip3-QDot to the path was extracted by calculating the angle between the projection vector (the vector from the path to each data point with the shortest distance) and the tangent vector (the vector for each projection point in the direction of the spline).

Analysis of distributions with error estimation

For estimating parameters from any given distribution (e.g. velocity, rotational pitch, rates) we used a bootstrapping approach (13, 14). Here, the distribution (*N* number of measurements) was resampled by randomly picking *N* measurements from the measured distribution (with replacement) and calculating the median of the resampled distribution. This was repeated 1000 times. The resulting bootstrapping distribution was used to estimate the parameter (mean of the bootstrapping distribution μ) and its error (standard deviation of the bootstrapping distribution σ). All values and errors as well as error bars in this paper use $\mu \pm 3\sigma$ (99% confidence interval), unless otherwise noted.

Calculation of stepping parameters

Double-stabilized microtubules used in the experiment have a lefthanded supertwist with a pitch of $\Psi_0 = 8.4\,\mu$m (7), a tubulin interdimer distance of $d_{\text{step}} = 8.3\ \text{nm}$ (15) and 14 protofilaments. Motor proteins that would not change protofilaments (e.g. kinesin-1) would then slightly rotate to the left in order to complete a full rotation within 8.4 μm. The angle per step can then be calculated as $\theta_{\text{step}} = 360^\circ / N_{\text{steps}} = 360^\circ/(8400/8.3) = 0.36^\circ$. For Kip3, the number of forward steps N_{steps} per full rotation (rotational pitch $\Psi_{\text{Kip3}} = 1.9\,\mu$m) is much lower ($N_{\text{steps}} = \Psi_{\text{Kip3}}/d_{\text{step}} = 1900/8.3 = 229$) and the microtubule supertwist would only account for 82° of the rotation ($N_{\text{steps}} \cdot \theta_{\text{step}}$). The remaining 278° must be attributed to sidestepping. Since 14 PF would yield a $\theta_{\text{PF}} = 360^\circ/14 = 26^\circ$ for each protofilament switch, Kip3 must switch protofilaments $N_{\text{switch}} = 278^\circ/\theta_{\text{PF}} = 278^\circ/26 = 11$ times while it takes 229 forward steps. This yields an effective sidestepping probability per forward step of 5 % (one sidestep per 21 forward steps). The effective sidestepping rate $k_{\text{sidestep}} = N_{\text{switch}} \cdot v_{\text{Kip3}}/\Psi_{\text{Kip3}}$ where v_{Kip3} is the forward velocity of Kip3. In summary, the effective sidestepping probability per forward step and the effective sidestepping rate can be calculated from the rotational pitch Ψ_{Kip3} (given in nm) and velocity v_{Kip3} (given in nm/s) by:

$$P_{\text{sidestep}} = \frac{N_{\text{switch}}}{N_{\text{steps}}} = \frac{14\, d_{\text{step}}\left(1-\Psi_{\text{Kip3}}/\Psi_0\right)}{\Psi_{\text{Kip3}}};\ d_{\text{step}} = 8.3\ \text{nm}\ \&\ \Psi_0 = 8400\ \text{nm}$$

$$k_{\text{sidestep}} = N_{\text{switch}}\frac{v_{\text{Kip3}}}{\Psi_{\text{Kip3}}} = \frac{14\, v_{\text{Kip3}}\left(1-\Psi_{\text{Kip3}}/\Psi_0\right)}{\Psi_{\text{Kip3}}};\ \Psi_0 = 8400\ \text{nm}$$

Further, the forward stepping rate k_{forward} and dwell time per forward step t_{step} can be calculated from the velocity v_{Kip3} by:

$$k_{\text{forward}} = \frac{v_{\text{Kip3}}}{d_{\text{step}}}$$

$$t_{\text{step}} = \frac{1}{k_{\text{forward}}}$$

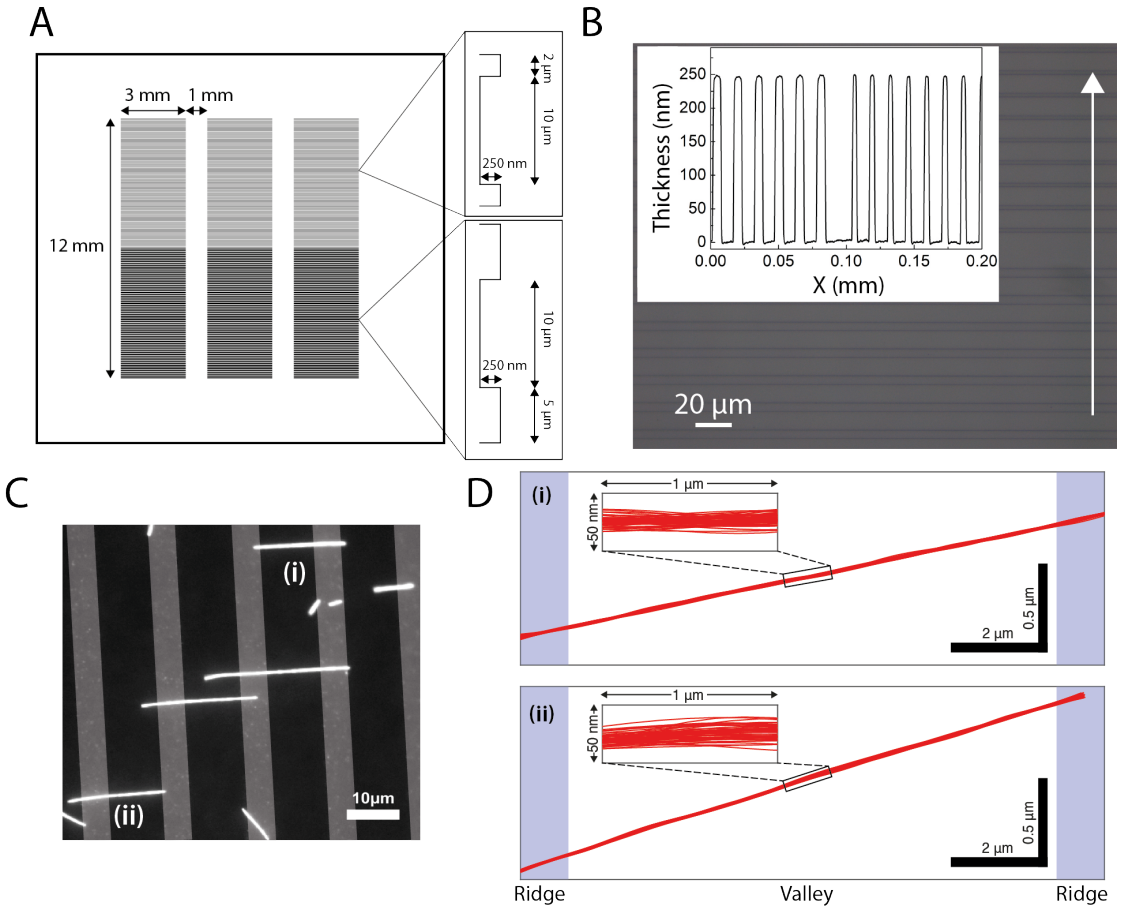

Figure S1 – Microtubules suspended on polymer ridges structured on glass using UV Nanoimprint Lithography (UV-NIL). (A) Glass coverslips were patterned with polymer resin using UV-NIL as described in the SI Appendix, Fabrication of polymer structures on glass. As seen in the illustration, the pattern imprinted on the glass coverslips had two different regions characterized by relief lines (that form the ridges) with a height of about 250 nm and a width respectively of 2 µm and 5 µm, separated by 10 µm (the valleys between the ridges). **(B)** Microscopy image of the polymer-patterned coverslip. Inset: The step height analysis of the polymer patterned coverslip obtained from profilometer measurement (X scan direction indicated by the white line; DektakXT, Bruker Nano GmbH, Karlsruhe, Germany). The ridges on the patterned coverslip have a smooth, blunt profile. **(C)** Fluorescent micrograph of rhodamine-labeled double-stabilized microtubules, freely-suspended by immobilizing them on the ridges of a polymer patterned coverslip via tubulin antibodies. The background intensity of the ridges has been enhanced to guide the eye. **(D)** Two-dimensional tracks of two suspended microtubules imaged for 50 frames [marked (i) and (ii) in (C)]. The localization precision of the tracked microtubules was 4.6 nm for (i) and 4.24 nm for (ii), indicating that the suspended microtubules were tautly bound and not swaying around.

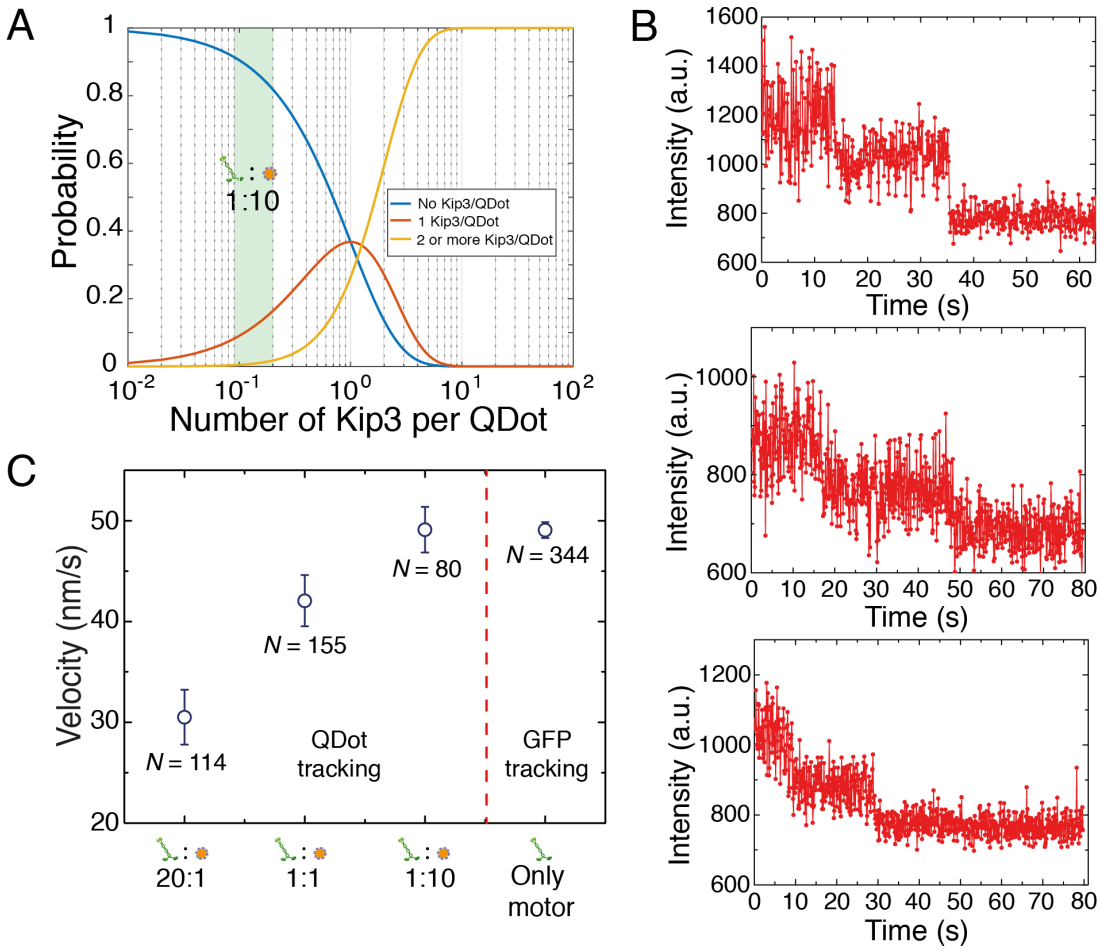

Figure S2 - Single molecule conditions for the Kip3-QDot conjugates: The Kip3 motors are tagged with a multifunctional GFP (mfGFP) tag, having a streptavidin binding peptide (SBP) inserted within the GFP sequence (16), that enables conjugation to streptavidin coated QDots. We confirmed single molecule conditions at the incubation ratio 1:10 (Kip3:QDot) by **(A)** considering the incubation stoichiometry of the motors and QDots; **(B)** direct observation of the number of motors attached to the QDot; **(C)** comparing the motility parameters of the QDot linked motor with single motors. **(A)** The probability of Qdots to be coupled to no Kip3, one Kip3 and two (or more) Kip3 according to Poisson statistics is plotted versus the stoichiometric ratio at which the Kip3 motors were incubated with QDots. At least 95 % of the Kip3-QDot conjugates have only one Kip3 motor at 1:10 Kip3:QDot mixing ratio(shaded in green). **(B)** The Kip3-QDot conjugates were stuck to microtubules using AMP-PNP in stepping assays. The GFP signals corresponding to majority of the Kip3-QDot conjugates (≈ 96 %; N = 45) showed 2-step photobleaching (or less) characteristic of a single Kip3 dimer as shown in the three examples. **(C)** Stepping velocity of Kip3-QDot conjugates at 20:1 (30.5 ± 3 nm/s; N = 115), 1:1 (42.1 ± 3 nm/s; N = 155) mixing ratio is much lower than single molecule velocity (49.1 ± 1 nm/s; N = 344). However, at 1:10 (49.1 ± 3 nm/s; N = 80) mixing ratio the Kip3-QDot velocity is not significantly different from single molecule velocity (P = 0.9, Mann-Whitney U test).

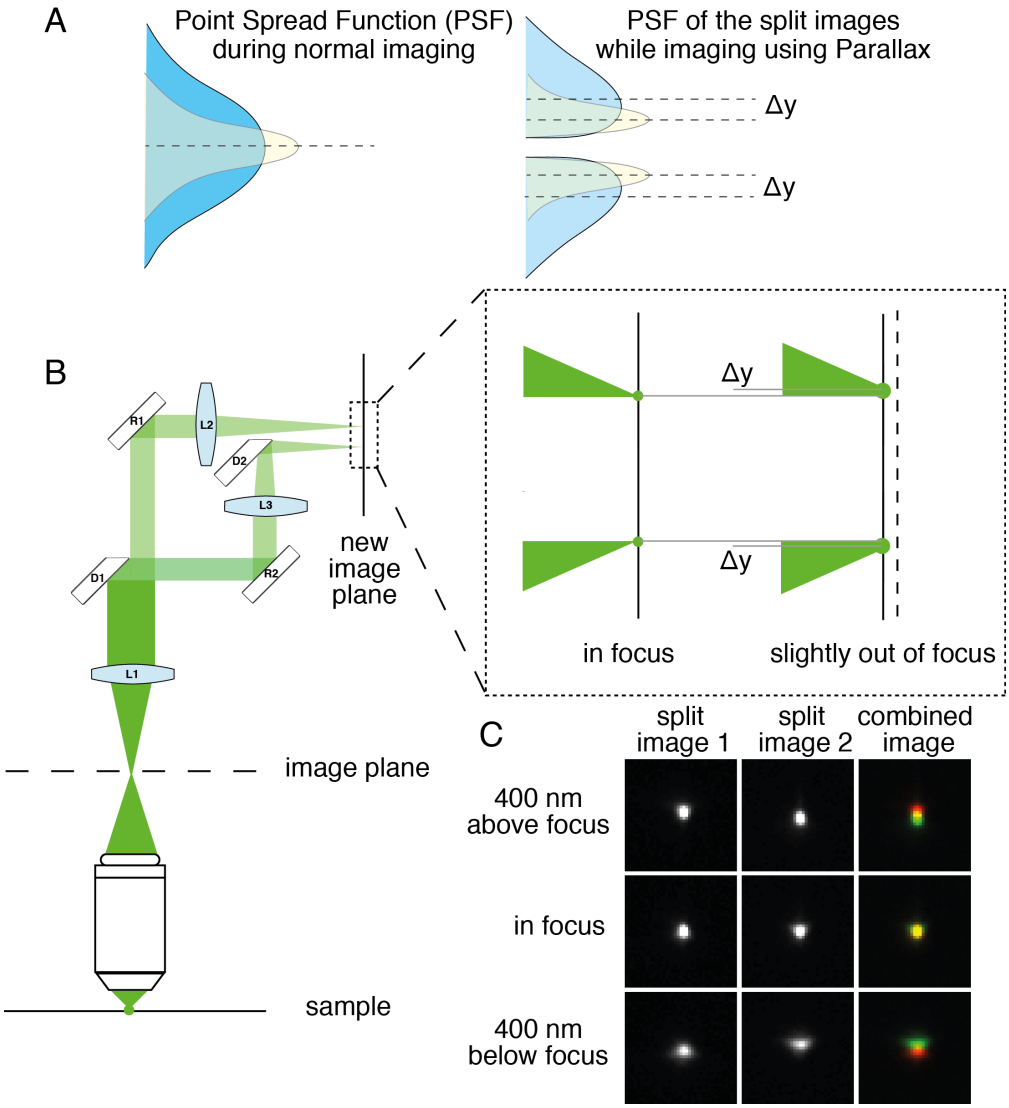

Figure S3 - 3D imaging using Parallax: (A) Illustration of the principle of Parallax. In case of a normal PSF for an object in focus (yellow in left image) a shift in z spreads the PSF (blue in left image) but does not change the central position. In Parallax, the PSF is split along the y-axis (or x-axis) into two asymmetric PSFs (yellow in right image). A shift along the z-axis in such a system leads to a relative shift in y between the central positions of the two split PSFs (blue in right image). Therefore, a relative shift Δy between the two split PSFs provide z information of the imaged object. (B) A schematic illustration of the Parallax set-up. A lens L1 placed one focal length away from the image collimates the emission signal from sample. This collimated beam is split by a D-shaped mirror D1 placed at the back focal plane. The two split beams are directed by mirrors R1, R2 and D2 and focused onto different parts of the same camera chip using image focusing lens L2 and L3. When sample moves slightly out of focus, the split images shift relative to each other (inset). (C) A 200 nm Tetraspeck bead imaged using Parallax. When the bead is in focus the two split images overlay on each other, as seen in the combined image. On moving the bead 400 nm above (below focus), the split images move towards (away) each other.

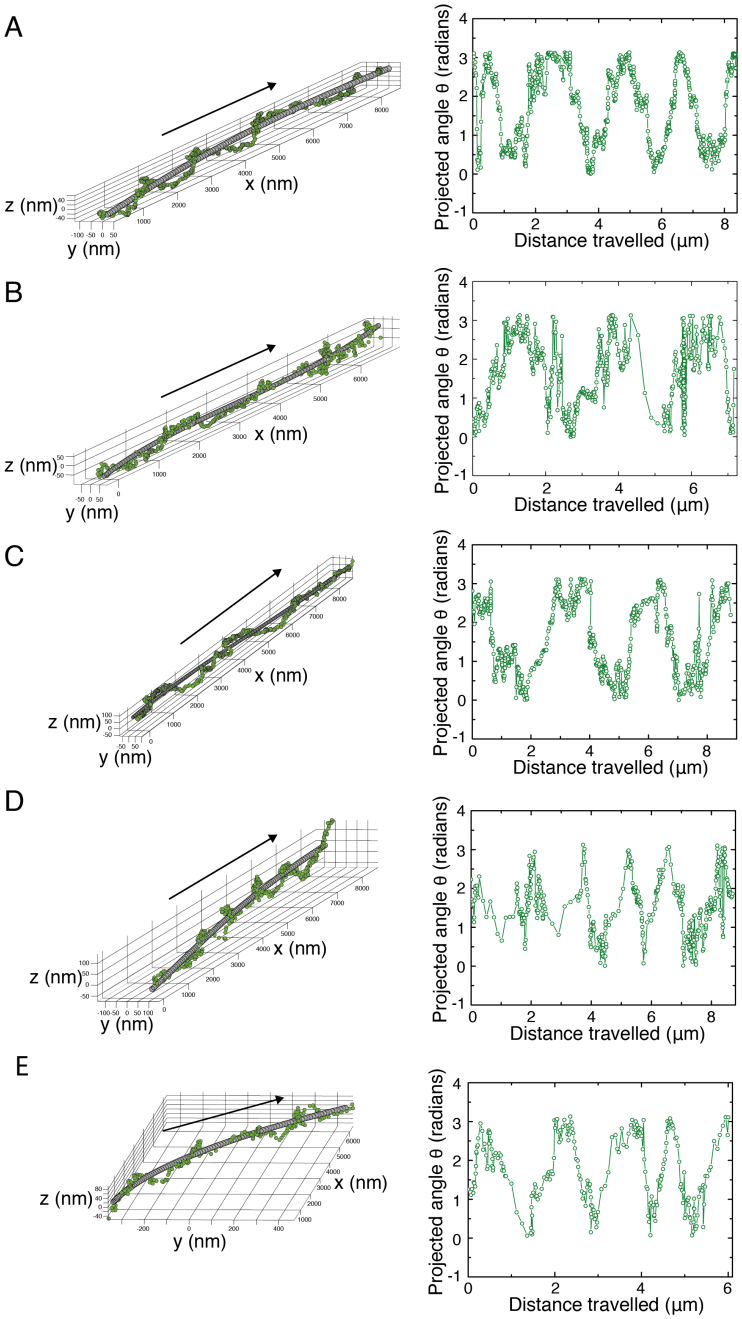

Figure S4 - Example Kip3-QDot stepping events on freely suspended microtubules: The 3-D tracking data around the fitted tube and plot of the angle projected by the Kip3-QDot to the fitted path versus the distance travelled for 5 example tracks. **(A)** Example event A has a velocity of 42.6 ± 1.0 nm/s and rotates with an average pitch of 2.1 ± 0.2 μm (number of rotations n = 3). **(B)** Example event B has a velocity of 43.2 ± 11.0 nm/s and rotates with an average pitch of 2.3 ± 0.3 μm (n = 2). **(C)** Example event C has a velocity of 50.1 ± 0.1 nm/s and rotates with an average pitch of 2.7 ± 0.4 μm (n = 2). **(D)** Example event D has a velocity of 39.4 ± 2.1 nm/s and rotates with an average pitch of 1.6 ± 0.2 μm (n = 4). **(E)** Example event E has a velocity of 40.0 ± 4.5 nm/s and rotates with an average pitch of 1.4 ± 0.4 μm (n = 3).

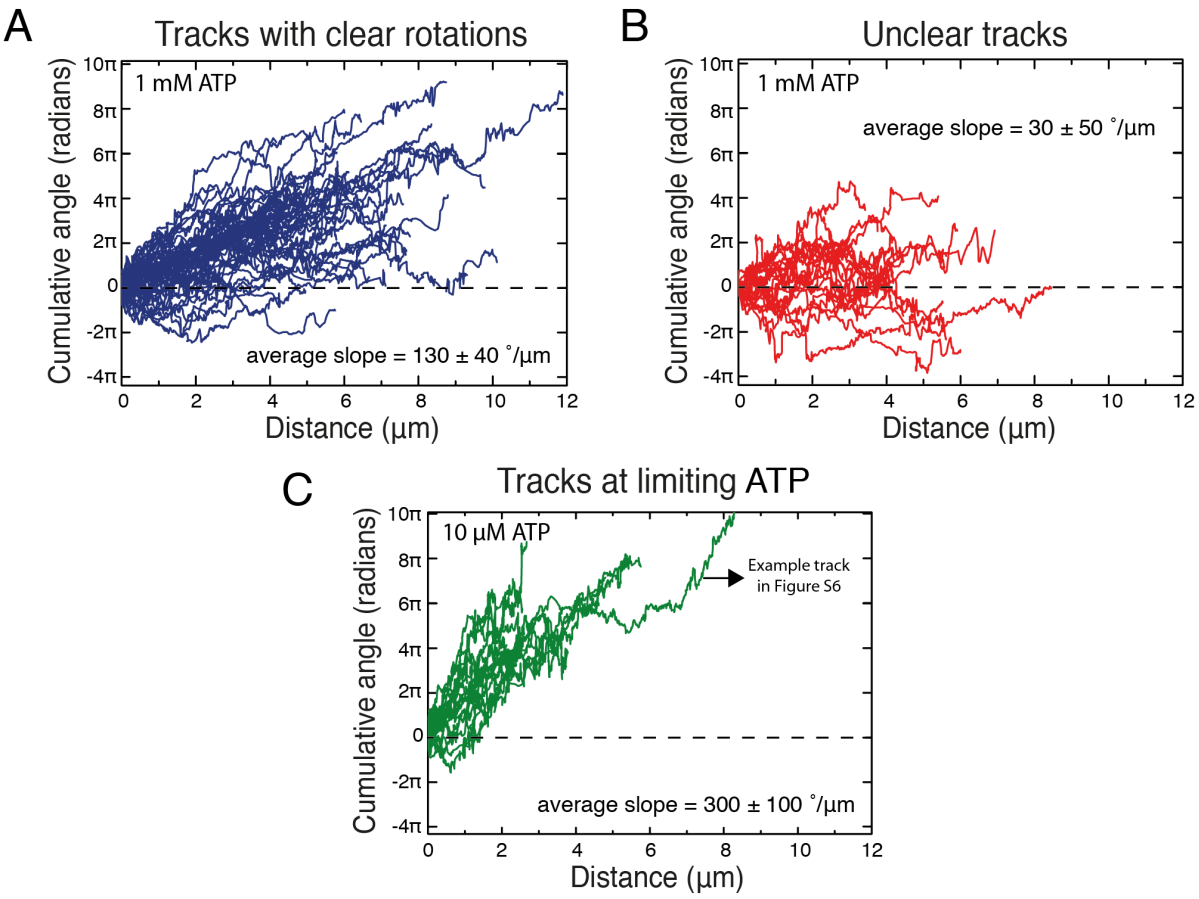

Figure S5 – Cumulative plots for all analyzed Kip3-QDot stepping events on freely suspended microtubules: (A) Cumulative angles for all the 50 events at 1mM ATP that showed clear rotations plotted versus the linear distance travelled. All the events show left-handed rotation around the fitted tube in the direction of motion with an average slope of 130 ± 40 °/ µm. **(B)** Cumulative angles for all the 23 unclear events at 1mM ATP plotted versus the distance travelled. The unclear events also have a leftward bias, though less pronounced (average slope = 30 ± 50 °/µm). **(C)** Cumulative angles for all the 19 events at 10 µM ATP that showed clear rotations plotted versus the distance travelled. The events have shorter left-handed rotational pitches in comparison to events at 1mM ATP (average slope = 300 ± 100 °/µm).

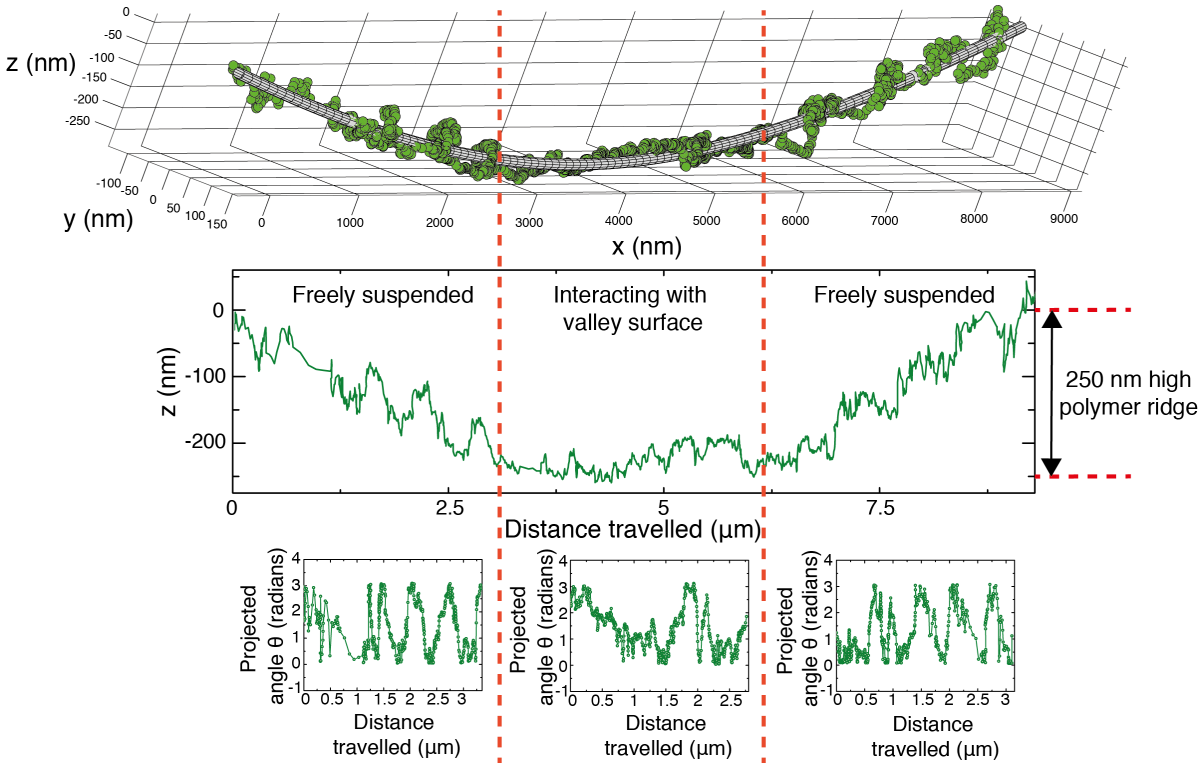

Figure S6 – 3D motility of Kip3 is hindered on surface interacting microtubules: 3-D tracking data around the fitted tube for an example Kip3-QDot event at 10 µM ATP. Plot of the z-coordinate versus the forward distance travelled indicates that the template microtubule for the Kip3-QDot event is freely suspended at the ends but touches the valley surface in the middle. The track is split into 3 sections indicated by the red dotted lines. The Kip3-QDot rotates freely in the first suspended section as indicated by the 3-D tracking data around the fitted tube and plot of the projected angle with linear distance travelled. The pitch is 0.68 ± 0.07 µm, and the average distance of the Kip3-QDot track from the fitted tube surface is 19.5 nm. The rotational motion of the Kip3-QDot is restricted in the second section where the microtubule interacts with the surface as indicated by the 3-D tracking data around the fitted tube and plot of the projected angle with linear distance travelled. The average distance of the Kip3-QDot track from the fitted tube surface is 9.4 nm. The Kip3-QDot rotates freely in the third suspended section as indicated by the 3-D tracking data around the fitted tube and plot of the projected angle with linear distance travelled. The pitch is 0.66 ± 0.07 µm, and the average distance of the Kip3-QDot track from the fitted tube surface is 15.3 nm.

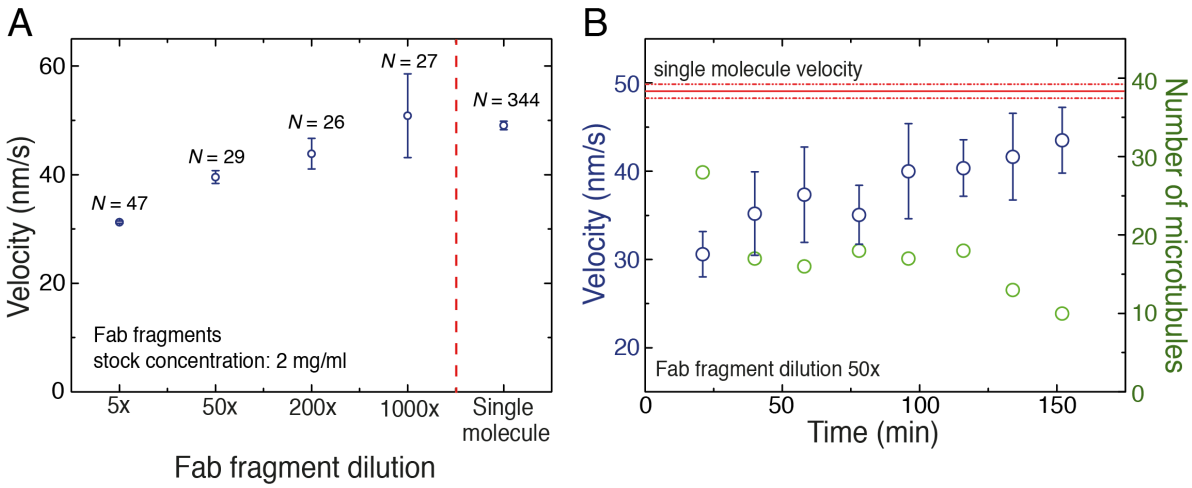

Figure S7 – Velocity of microtubules gliding on Kip3 depends on the density of motors: (A) The velocity of microtubules gliding on Kip3 varies with density of Kip3 motors attached to the substrate. The figure shows the MT gliding velocity for different Fab fragment dilutions (31.2 ± 1nm/s at 5x, 39.6 ± 1nm/s at 50x, 43.8 ± 3nm/s at 200x and 51.0 ± 8nm/s at 1000x dilution; Fab fragment stock concentration– 2 mg/ml). The Fab fragment concentration determines the Kip3 motor density on the surface. The gliding velocity increases on reducing number of motors on the surface with almost single molecule velocity (measured in stepping assays; velocity = 49.1 ± 1nm/s; N=344) at 1000x dilution (though MT gliding is very poor with high fluctuations at low densities). **(B)** Gliding velocity plotted over time for Kip3 gliding assay at 50x Fab fragment dilution. The gliding velocity is much lower than the single molecule velocity but increases over time. The decrease in the number of gliding MTs per field of view (green points) indicates a reduction in the effective density of motors with time.

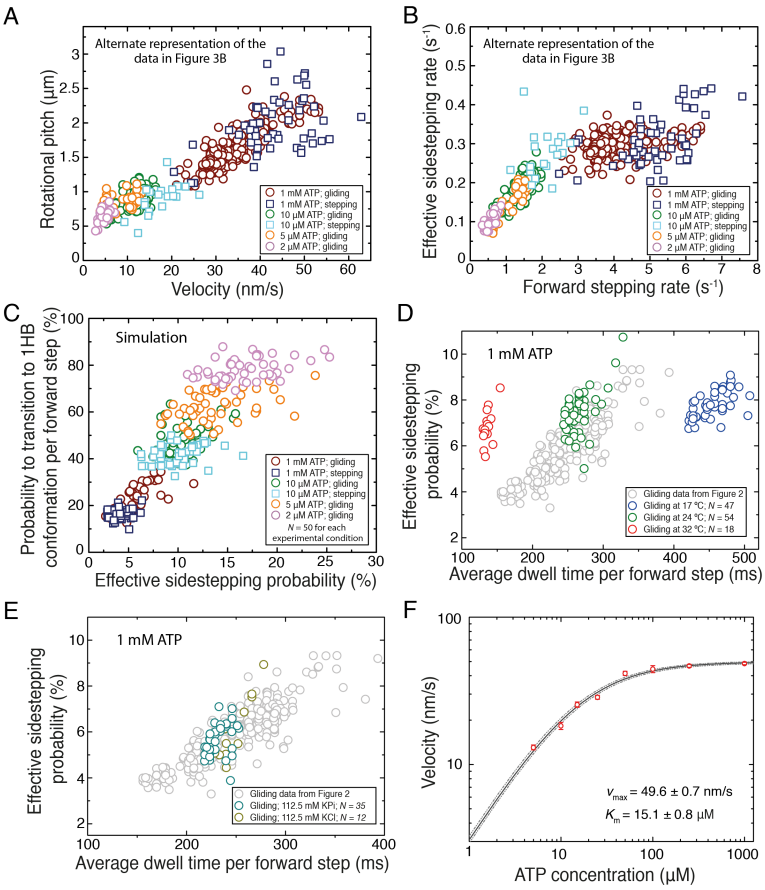

Figure S8 – Further data with regard to the sidestepping mechanism of Kip3: (A) Rotational pitches in dependence of the forward velocity for Kip3-QD tracks and microtubules in Kip3 gliding assays, at different ATP concentrations. **(B)** Effective sidestepping rate plotted against the forward stepping rate for Kip3-QD tracks and microtubules in Kip3 gliding assays at different ATP concentrations. (A) and (B) are alternate representation of the data shown in Fig. 3B. **(C)** Probability to transition to the 1HB conformation (ATP waiting state) per forward step increases linearly with an increase in the effective sidestepping probability per forward step in the simulation for gliding assays and stepping assays, at different ATP conditions. 50 events were simulated for each experimental condition. **(D)** Gliding rotation assays were performed at 17 °C (blue), 24 °C (green) and 32 °C (red). While the average dwell time per forward step varied substantially (453 ± 19 ms at 17 °C, 262 ± 10 ms at 24 °C and 135 ± 5 ms at 32 °C) there was only a marginal increase in effective sidestepping probability per forward step on decreasing temperature (6.8 ± 0.5 % at 17 °C, 7.5 ± 0.4 % at 24 °C and 7.7 ± 0.3 % at 32 °C). Gliding data from Fig. 2B is plotted in grey for reference. **(E)** Gliding rotation assays were performed in assay buffer with additional P_i (BRB80 with 112.5 mM KP_i) followed by exchange of the normal assay buffer (BRB80 with 112.5 mM KCl). Both, the average dwell time per forward step (230 ± 10 ms in buffer with KP_i and 244 ± 22 ms in buffer with KCl, $P = 0.012$) and the effective sidestepping probability per forward step (5.8 ± 0.7% in buffer with KP_i and 5.7 ± 1.8 % in buffer with KCl, $P = 0.913$) do not change significantly in the buffer with additional P_i. **(F)** Dependence of Kip3 stepping velocity with ATP concentration. The Kip3 stepping velocity varies with ATP concentration (plotted logarithmically) according to Michelis-Mentis kinetics, yielding a maximum stepping velocity v_{max}= 49.7 ± 0.4 nm/s and k_m = 15.2 ± 0.5 µM. Each data point in the graph represents the 90-350 stepping events.

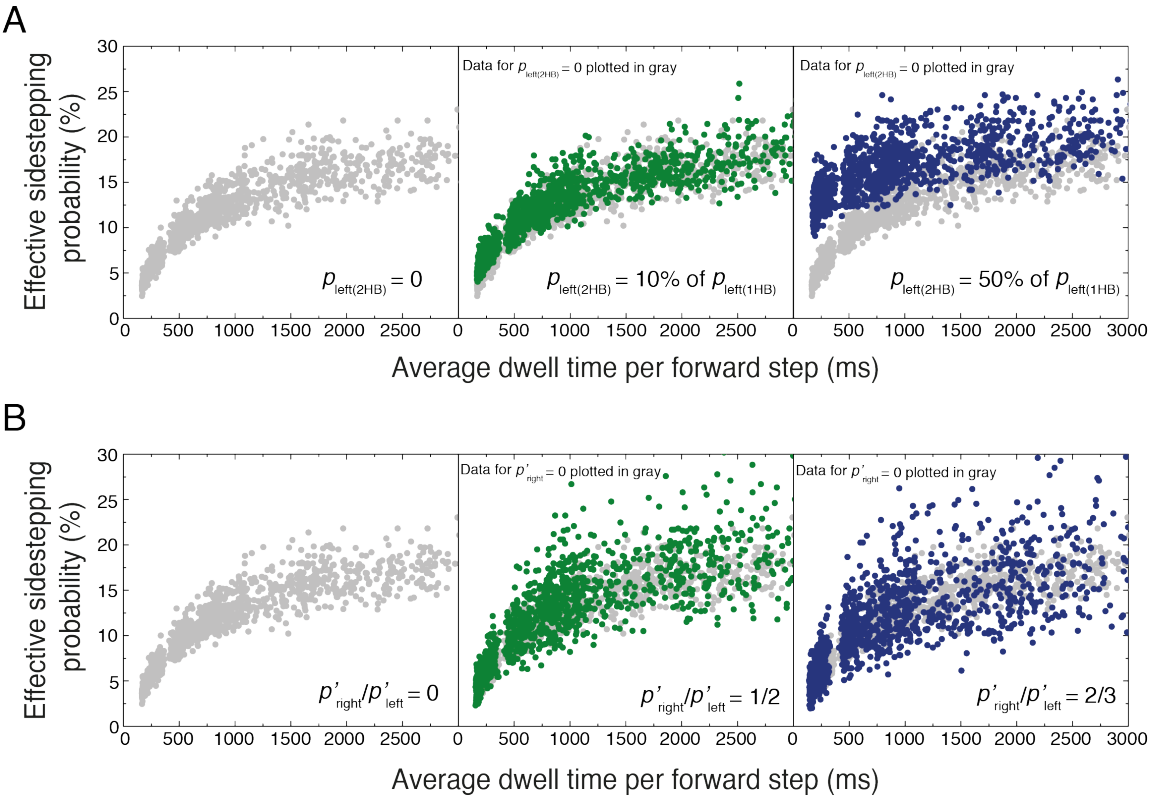

Figure S9 – Extensions to the model for the sidestepping mechanism of Kip3. (A) Numerical simulations assuming that Kip3 also sidesteps with a basal probability $p_{\mathrm{left(2HB)}}$ when binding ATP in the 2HB conformation. The simulated effective sidestepping probability per forward step is plotted in dependence of the average dwell time per forward step (300 molecules each at 1000 µM, 10 µM, 5 µM and 2 µM ATP; all in the same color) for $p_{\mathrm{left(2HB)}} = 0$ (left panel; gray circles), $p_{\mathrm{left(2HB)}} = 0.018$ (middle panel; green circles), $p_{\mathrm{left(2HB)}} = 0.09$ (right panel; blue circles). The other simulation parameters are the same as given in Table S1. This extension to the model can fit the experimental data in Fig. 3B only if $p_{\mathrm{left(2HB)}}$ is small (< 10% of $p_{\mathrm{left(1HB)}}$). **(B)** Numerical simulations assuming that Kip3 performs both leftward and rightward sidesteps with the probabilities p'_{left} and p'_{right}, respectively, such that $p_{\mathrm{left}} = p'_{\mathrm{left}} - p'_{\mathrm{right}}$ (> 0) provides the observed leftward bias. The simulated effective sidestepping probability per forward step is plotted in dependence of the average dwell time per forward step (300 molecules each at 1000 µM, 10 µM, 5 µM and 2 µM ATP; all in the same color) for $p'_{\mathrm{right}}/p'_{\mathrm{left}} = 0$ (left panel; gray circles), $p'_{\mathrm{right}}/p'_{\mathrm{left}} = 1/2$ (middle panel; green circles), $p'_{\mathrm{right}}/p'_{\mathrm{left}} = 2/3$ (right panel; blue circles). For different ratios of $p'_{\mathrm{right}}/p'_{\mathrm{left}}$, the simulation parameters (p'_{left}, t_{step} and $k_{\mathrm{2HB\rightarrow 1HB}}$) are adjusted to best fit the experimental data in Fig. 3B. For $p'_{\mathrm{right}}/p'_{\mathrm{left}} = 0$ simulation parameters are the same as given in Table S1; for $p'_{\mathrm{right}}/p'_{\mathrm{left}} = 1/2$, $p'_{\mathrm{left}} = 0.28$, $t_{\mathrm{step}} = 140$ ms and $k_{\mathrm{2HB\rightarrow 1HB}} = k_{\mathrm{ATP(max)}}/3$; for $p'_{\mathrm{right}}/p'_{\mathrm{left}} = 2/3$, $p'_{\mathrm{left}} = 0.30$, $t_{\mathrm{step}} = 120$ ms and $k_{\mathrm{2HB\rightarrow 1HB}} = k_{\mathrm{ATP(max)}}/2$. This extension to the model can fit the trend observed in the experimental data in Fig. 3B but the variance in the effective sidestepping probability for individual motors increases upon increasing the ratio of rightward steps to leftward steps.

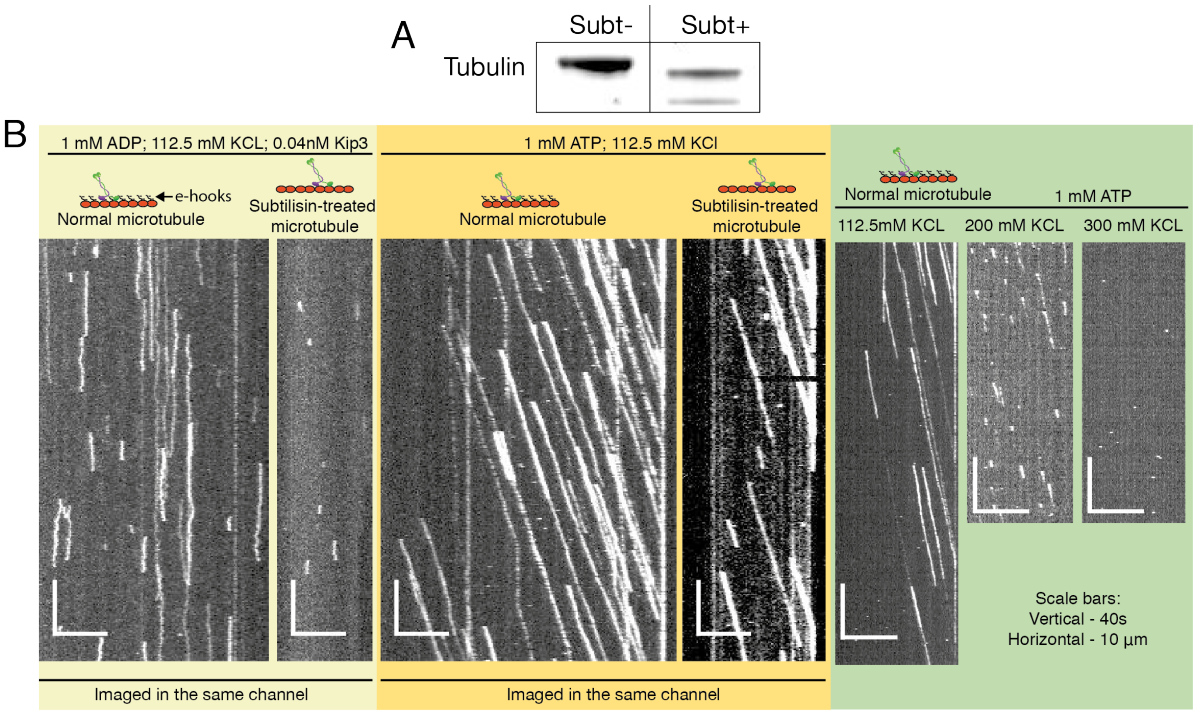

C

Number	Nucleotide (1 mM)	Microtubule Treatment	Salt conc. (mM)	Velocity (nm/s)	Runlength (nm)	Interaction time (s)	On-rate (events/µm*s)
308	ADP	Normal	112.5	-	-	4.6 ± 0.7	30.6
118	ADP	Subtilisin treated	112.5	-	-	0.8 ± 0.2	7.7
56	ATP	Normal	112.5	54.4 ± 3	3068 ± 1024	56 ± 18	-
62	ATP	Subtilisin treated	112.5	49.2 ± 4	1474 ± 356	29 ± 8	-
92	ATP	Normal	112.5	47 ± 2	2273 ± 642	47 ± 14	-
118	ATP	Normal	200	57 ± 2	357 ± 68	6 ± 2	-
51	ATP	Normal	300	63 ± 7	73 ± 24	1.2 ± 0.4	-

Figure S10 – Single-molecule properties of Kip3 change on subtilisin-treated microtubules and on increasing salt concentration: (A) SDS gel performed to verify cleavage of microtubule e-hooks. 'Subt+' indicates subtilisin treated microtubules and 'Subt-' indicates non-treated control microtubules. **(B)** Example kymographs of Kip3 motors on different microtubules (subtilisin-treated and normal microtubules), in different nucleotide states (ADP and ATP) and with different salt conditions in the assay buffer (112.5 mM KCl, 200 mM KCl and 300 mM KCl). Subtilisin-treated and normal microtubules were immobilized in the same flow channel. Vertical scale bars represent 40 s and horizontal scale bars represent 10 μm. **(C)** Table indicating the motility parameters obtained for Kip3 motors in different experimental conditions. On-rates provide relative comparison between subtilisin-treated and normal microtubules as the values depend on the concentration of Kip3 in solution. The runlengths and interaction times are likely underestimated, especially for experimental conditions providing long interaction times, because a large percentage of Kip3 motors bleached or reached the microtubule plus-ends.

Simulation Parameter	Value
$t_{\mathrm{step(max)}}$	160 ms (at 1mM ATP)
$t_{\mathrm{waiting\,ATP(max)}}$	115 ms (at 1mM ATP)
t_{rest}	45 ms (independent of [ATP])*
d_{step}	8.3 nm
K_{M}	15 μM
$t_{\mathrm{step}}([\mathrm{ATP}])$	$t_{\mathrm{step(max)}} \cdot ([\mathrm{ATP}] + K_{\mathrm{M}})/[\mathrm{ATP}]$
$k_{\mathrm{ATP}}([\mathrm{ATP}])$	$1/(t_{\mathrm{step}}([\mathrm{ATP}]) - t_{\mathrm{rest}})$
$k_{\mathrm{ATP(max)}}$	8.70 s^{-1} (at 1mM ATP)
$k_{\mathrm{2HB\rightarrow 1HB}}$	2.18 s^{-1} (on normal microtubules)* 4.35 s^{-1} (on subtilisin treated microtubules)* 5.44 s^{-1} and 8.70 s^{-1} (200 mM and 300 mM KCl in assay buffer, respectively)
p_{left}	18 %
p_{futile}	0 - 20 % (for stepping events)* 0 - 60 % (for gliding events)* 20 - 45 % (for subtilisin treated microtubule gliding events)* 10 – 35 % and 25 – 50 % (for gliding events in assay buffer with 200 mM and 300 mM KCl, respectively)

*estimated from best fit to experimental data

Table S1 - Parameters of the numerical simulation using the proposed model. The dwell time $t_{\mathrm{step(max)}}$ at physiological ATP conditions was determined by fitting the dependence of the velocity on ATP concentration with Michalis-Menden-kinetics (Fig. S8F). We adjusted the dwell time of the ATP hydrolysis $t_{\mathrm{hydrolysis}}$ in order to get a similar slope as in Fig. 2B. While t_{rest} is not affected by ATP concentration, $t_{\mathrm{step}}([\mathrm{ATP}])$ and $t_{\mathrm{waiting\,ATP}}([\mathrm{ATP}])$ change with decreasing ATP concentration. The average dwell time per forward step at different ATP concentrations was calculated with the estimated K_{M} from control Kip3 stepping assays (Fig. S8F). The ATP binding rate is then estimated for the different ATP concentrations, while the transition rate from the 2HB to the 1HB conformation $k_{\mathrm{2HB\rightarrow 1HB}}$ was kept constant since we assume a nucleotide-independent transition. The simulations for gliding events with subtilisin-treated microtubules and for gliding events in high salt conditions used an increased transition rate $k_{\mathrm{2HB\rightarrow 1HB}}$ due to a weaker interaction of the ADP bound motor with the microtubule (Fig. S9B and S9C). The probability p_{left} can be estimated from the saturating effective sidestepping probability at limiting ATP conditions (see Fig. 3B) and we added a probability for futile steps p_{futile} to account for the experimentally observed velocity variations, which might be due to stochastic nature of the motor in stepping assays and multi-motor effects in gliding assays (Fig. S7).

MATLAB code for numerical simulation of the stepping mechanism

```
function Kip3Simulation
% States: % 1 = 2HB waiting for ATP, 2 = 1HB waiting for ATP, 3 = ATP hydrolysis
rng('shuffle');
% motor and MT properties
t_step_max = 0.160; % time per step in s, 6.25 steps per second (51.9nm/s)
k_step_max = 1 / t_step_max;
t_rest = 0.045; % time per ATP independent state
k_rest = 1 / t_rest;
k_ATP_max = 1 / (t_step_max - t_rest);
k_2HBto1HB = k_ATP_max / 4; % transition rate from 2HB to 1HB
Km = 15; % Michaelis-Menten constant in µM
p_left = 0.18; % probability of sidestepping in 1HB
maxFutile = 0.4; % maximum probability of futile hydrolysis
minFutile = 0.2; % maximum probability of futile hydrolysis
kin1_pitch = 8400; % rotational pitch of 14-PF MTs gliding on kinesin-1
d_step = 8.3; % forward stepsize of kinesin motors
rot_perForwardStep = 360 / (kin1_pitch / d_step);
rot_perSideStep = 360 / 14;
% simulation properties
nMol = 50; % number of molecules
ATP = 1000; % ATP concentration in µM
nRotations = 2; % number of rotations to average
T = 4000; % max time per molecule
dt = 0.001; % time resolution
% initialisation
itime = zeros(nMol,1);
pitch = zeros(nMol,1);
for n = 1:nMol
    % initialisation
    nForwardStep = 0;
    nSideStep = 0;
    rotation = 0;
    state = 1;
    % calculate rates and probabilities for specific ATP concentration
    k_step = k_step_max * ATP / (Km + ATP);
    t_step = 1 / k_step;
    k_ATP = 1 / (t_step - t_rest);
    p_ATP = k_ATP * dt;
    p_rest = k_rest * dt;
    p_2HBto1HB = k_2HBto1HB * dt;
    % calculate probabilities per motor
    p_futile = minFutile + rand*(maxFutile-minFutile);
    % start Monte-Carlo-Simulation
    for t = dt:dt:T
        if state == 1 % 2HB waiting for ATP
            p = rand;
            if p<p_ATP*(1-p_futile) % ATP binds in 2HB waiting state
                state = 3; % transition to ATP hydrolysis
                nForwardStep = nForwardStep + 1; % makes a forward step
                % adds rotation according to supertwist of 14-PF MTs
                rotation = rotation + rot_perForwardStep;
            elseif p>=p_ATP && p<p_2HBto1HB+p_ATP % transition to 1HB before ATP binding
                state = 2; % transition to 1HB waiting for ATP
            end
        end
        if state == 2 % 1HB waiting for ATP
            p = rand;
            if p<p_ATP*(1-p_futile) % ATP binds in 1HB waiting state
                state = 3; % transition to ATP hydrolysis
                p = rand;
                if p<p_left  % make sidestep after ATP binding
                    nSideStep = nSideStep+1; % makes a sidestep
                    % adds rotation according to switch of protofilament
                    rotation = rotation + rot_perSideStep;
                else  % make forward step after ATP binding
                    nForwardStep = nForwardStep+1; % makes a forward step
                    % adds rotation according to supertwist of 14-PF MTs
                    rotation = rotation + rot_perForwardStep;
                end
            end
        end
        if state == 3 % ATP hydrolysis and rest of the cycle
            p = rand;
            if p<p_rest % finishing rest of cycle
                % hydrolyse ATP, release ADP from leading head,
                % followed by Pi release from trailing head
                state = 1;
            end
        end
        if rotation > nRotations*360 % check if rotations are complete
            % average over all rotations
            itime(n,1) = t / nRotations;
            pitch(n,1) = nForwardStep * d_step / nRotations;
            break;
        end
    end
end
velocity = pitch./itime;
scatter(velocity,pitch/1000,100,'b','o','LineWidth',2,'MarkerFaceColor','white');
```

SI Appendix References

1. Nitzsche B, et al. (2010) *Studying kinesin motors by optical 3D-nanometry in gliding motility assays.* (Elsevier). First edit doi:10.1016/S0091-679X(10)95014-0.
2. Sun Y, McKenna JD, Murray JM, Ostap EM, Goldman YE (2009) Parallax: high accuracy three-dimensional single molecule tracking using split images. *Nano Lett* 9(7):2676–82.
3. Ruhnow F, Zwicker D, Diez S (2011) Tracking single particles and elongated filaments with nanometer precision. *Biophys J* 100(11):2820–8.
4. Varga V, Leduc C, Bormuth V, Diez S, Howard J (2009) Kinesin-8 Motors Act Cooperatively to Mediate Length-Dependent Microtubule Depolymerization. *Cell* 138(6):1174–1183.
5. Tokunaga M, Imamoto N, Sakata-Sogawa K (2008) Highly inclined thin illumination enables clear single-molecule imaging in cells. *Nat Methods* 5(2):159–61.
6. Castoldi M, Popov A V (2003) Purification of brain tubulin through two cycles of polymerization-depolymerization in a high-molarity buffer. *Protein Expr Purif* 32(1):83–8.
7. Mitra A, Ruhnow F, Nitzsche B, Diez S (2015) Impact-free measurement of microtubule rotations on kinesin and cytoplasmic-dynein coated surfaces. *PLoS One* 10(9). doi:10.1371/journal.pone.0136920.
8. Korten T, et al. (2011) Fluorescence imaging of single Kinesin motors on immobilized microtubules. *Methods Mol Biol* 783:121–37.
9. Nitzsche B, Ruhnow F, Diez S (2008) Quantum-dot-assisted characterization of microtubule rotations during cargo transport. *Nat Nanotechnol* 3(9):552–556.
10. Hawkins TL, Sept D, Mogessie B, Straube A, Ross JL (2013) Mechanical properties of doubly stabilized microtubule filaments. *Biophys J* 104(7):1517–1528.
11. Ruhnow F, Kloβ L, Diez S (2017) Challenges in Estimating the Motility Parameters of Single Processive Motor Proteins. *Biophys J* 113(11):2433–2443.
12. Schneider CA, Rasband WS, Eliceiri KW (2012) NIH Image to ImageJ: 25 years of image analysis. *Nat Methods* 9(7):671–675.
13. Press WH, Teukolsky S a, Vetterling WT, Flannery BP (1992) *Numerical recipes in C (2nd ed.): the art of scientific computing* doi:10.2307/1269484.
14. McCabe GP, Moore DS (2006) *Introduction to the Practice of Statistics.* ed Freeman WH (New York). Vol. 5.
15. Zhang R, Alushin GM, Brown A, Nogales E (2015) Mechanistic origin of microtubule dynamic instability and its modulation by EB proteins. *Cell* 162(4):849–859.
16. Kobayashi T, et al. (2008) Engineering a novel multifunctional green fluorescent protein tag for a wide variety of protein research. *PLoS One* 3(12). doi:10.1371/journal.pone.0003822.